Supplementary Information

Positive and negative electrocaloric effect in direct and indirect characterization of $NaNbO_3$-based ceramics with tetragonal-cubic phase boundary

Hong Tao[1, 2], Jie Yin[2], Lin Zhao[1], Bo Wu[1], Jian Ma[1], Daji Ergu*[1], Jiagang Wu*[2]

[1]Sichuan Prov Key Lab Informat Mat, Southwest Minzu University, Chengdu 610041, China

[2]Department of Materials Science, Sichuan University, Chengdu 610064, China

*** Corresponding author:**

wujiagang0208@163.com and mswujg@scu.edu.cn (JG Wu)

ergudaji@163.com (D Ergu)

1. Structure analysis

Figure S1(a) shows the XRD patterns of the ceramics with x=0.15~0.18 when 2θ=20-70°. Perovskite structure without any impurity phase can be confirmed for all the ceramics. Combing with the well-matched Rietveld refinement results of XRD patterns with low Rw and Sig values [Fig. S1(b) and Table S1], the phase structure can be verified as: tetragonal for x=0.15, tetragonal-cubic multiphase coexistence for x=0.16-0.17, and pure cubic phase for x=0.18. With increasing x, tetragonal phase gradually decreases while cubic phase increases at room temperature [Table S1]. The specific lattice parameters are shown in Table S1. Dense solid solution with uniform grains is revealed in all the ceramics [Fig. S2]. And the phase images of virgin domain are obtained for the ceramics [Fig. S3]. When temperature increases to 60 °C, transformation from T phase to T&C multiphase coexistence happens for x=0.15, while pure T phase is obtained for x=0.16 [Fig. S4 and Table S2].

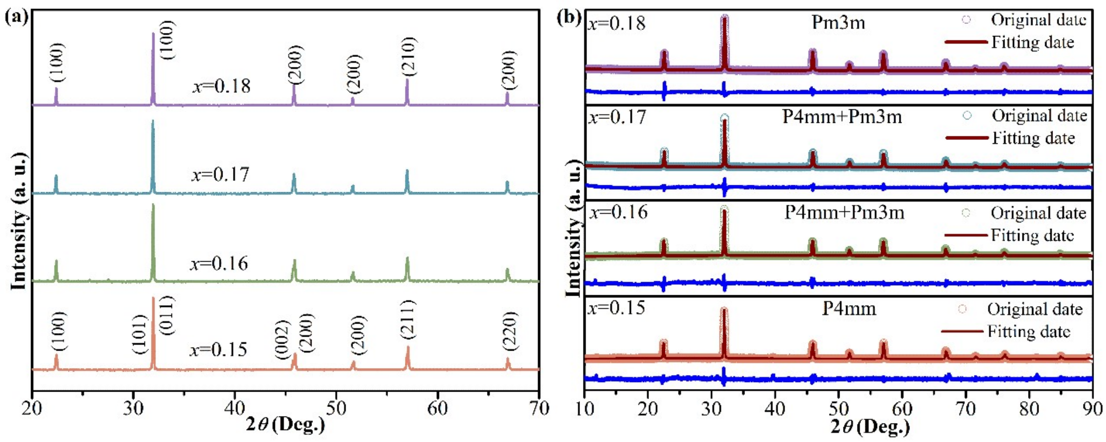

Figure S1. (a) room-temperature XRD patterns when 2θ=20-70° of the ceramics with different x, (b) the Rietveld refinement results of XRD patterns when 2θ=10-90°, measured at 25 °C.

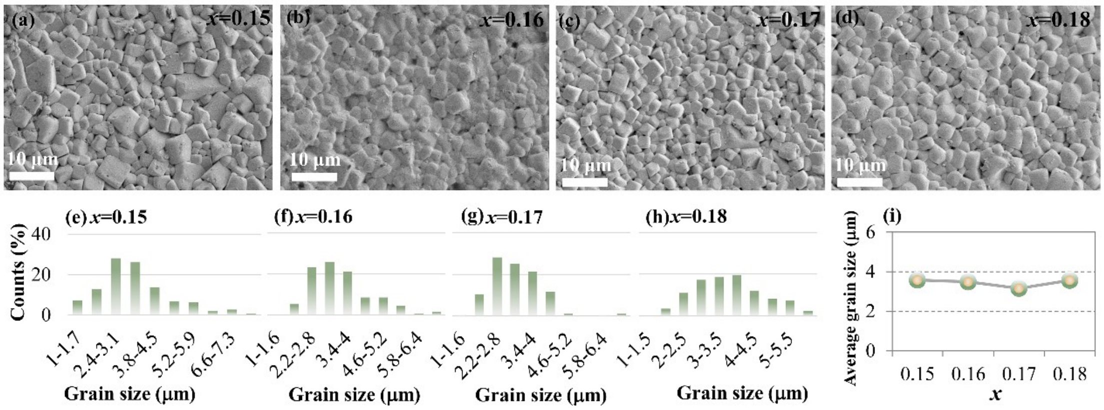

Figure S2. FE-SEM image of the ceramics with different *x*: (a) *x*=0.15, (b) *x*=0.16, (c) *x*=0.17, (d) *x*=0.18; distribution of grain size: (e) *x*=0.15, (f) *x*=0.16, (g) *x*=0.17, (h) *x*=0.18; (i) average grain size.

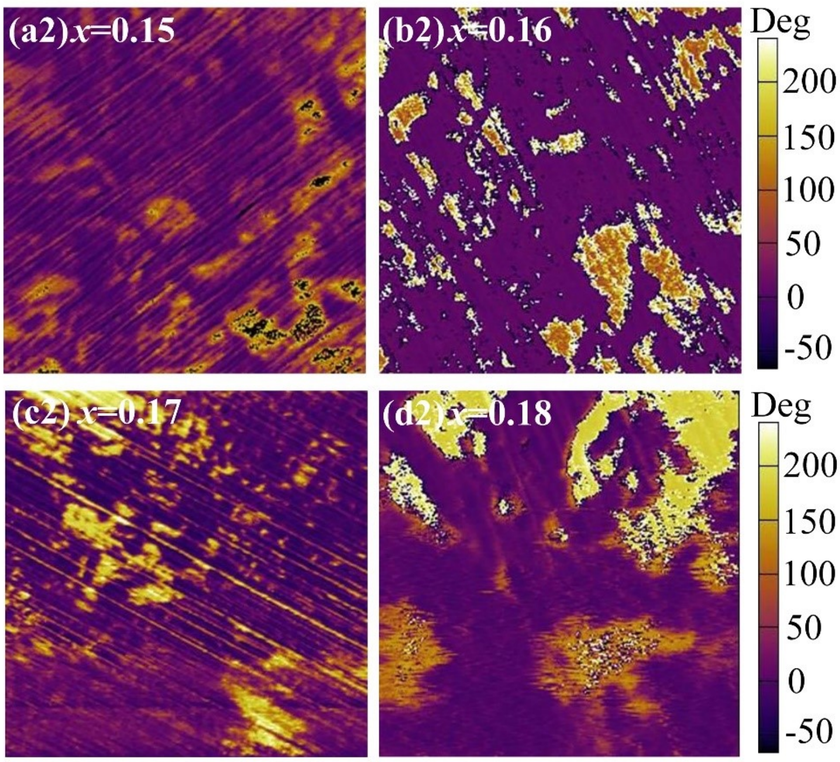

Figure S3. Phase images of virgin domain for the ceramics with different *x*: (a) *x*=0.15, (b) *x*=0.16, (c) *x*=0.17, (d) *x*=0.18.

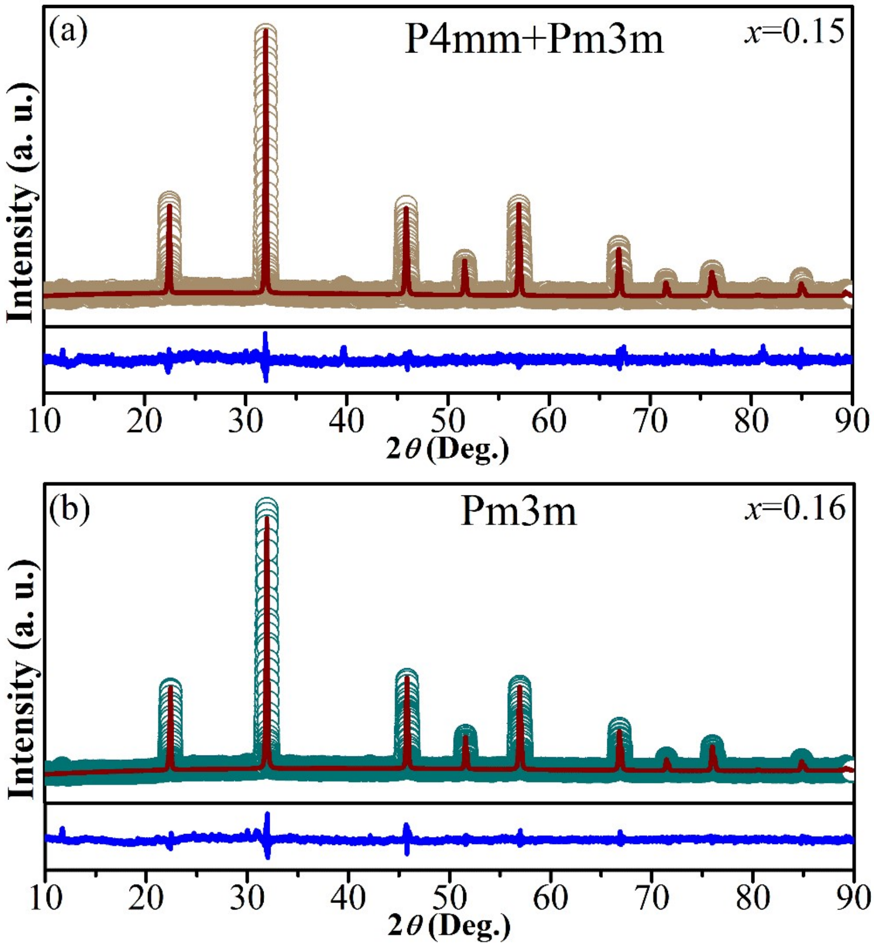

Figure S4. The Rietveld refinement results of XRD patterns when 2θ=10-90°, measured at 60 °C: (a) x=0.15, (b) x=0.16.

Table S1. Parameters of refine result for the NN-BZT ceramics with different compositions, measured at 25 °C.

x	Sig	R_w (%)	Space group	a (Å)	b (Å)	c (Å)	Alpha(°)
0.15	1.49	3.7	P4mm	3.9463	3.9463	3.9601	-
0.16	1.87	3.93	P4mm(50%)	3.9499	3.9499	3.9561	-
			Pm3m(50%)	3.7460	3.7460	3.7460	-
0.17	1.94	5.5	P4mm(10%)	3.9537	3.9537	3.9625	-
			Pm3m(90%)	3.9510	3.9510	3.9510	-
0.18	1.67	4.5	Pm3m	3.9538	3.9538	3.9538	-

Table S2. Parameters of refine result for the NN-BZT ceramics with different compositions, measured at 60 °C.

x	Sig	R_w (%)	Space group	a (Å)	b (Å)	c (Å)	Alpha(°)
0.15	1.50	3.7	P4mm(52%)	3.9512	3.9512	3.9527	-
			Pm3m(48%)	3.9514	3.9514	3.9514	-
0.16	1.69	3.6	Pm3m	3.9551	3.9551	3.9551	-

2. Ferroelectric properties

Figure S5(a)~(d) show the *P*-*E* loops under 40 kV/cm at different temperature. One can see the *P*-*E* loops gradually becomes slim with increasing temperature as P_r and E_C decrease. More importantly, the P_{max} shows an enhancement at 40~80 °C for *x*=0.15 and 30~60 °C for *x*=0.16 under 5~40 kV/cm [Fig, S5(e)~(h)]. And the enhancement is weakened under increasing electric field, which is due to more sufficient polarization under higher electric field. The phenomenon is on account of the contribution of PNRs to polarization. When *x*=0.17 and 0.18, the P_{max} shows obviously decreasing tendency with elevating temperature, originating from increased cubic phase and thermal disturbance.

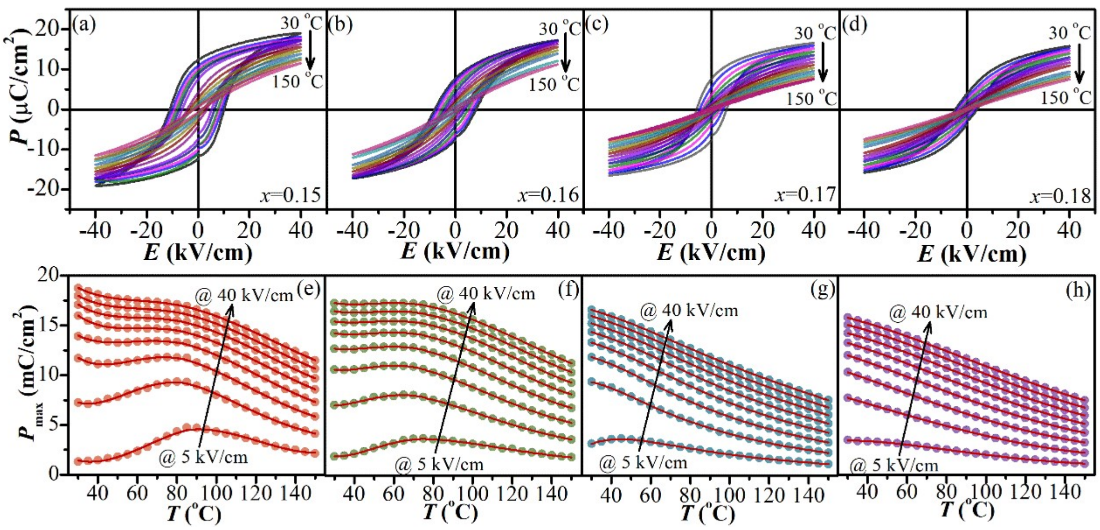

Figure S5. Temperature-dependent *P*-*E* loops at 30~150 °C 40 kV/cm: (a) *x*=0.15, (b) *x*=0.16, (c) *x*=0.17, (d) *x*=0.18; P_{max}-*T* curves at 5~40 kV/cm: (e) *x*=0.15, (f) *x*=0.16, (g) *x*=0.17, (h) *x*=0.18.